Electronic Supplementary Material (ESI) for Nanoscale.

Supplementary Materials for "Structural reconstruction and visible-light absorption versus internal electrostatic field in two-dimensional GaN-ZnO alloys"

Hanpu Liang[1] and Yifeng Duan[1, a)]

School of Materials and Physics, China University of Mining and Technology, Xuzhou, Jiangsu 221116, China

(Dated: 10 June 2021)

[a)]Electronic mail: yifeng@cumt.edu.cn

TABLE S1. Structure parameters of bulk haeckelite and wurtzite.

Structure	Phase	Parameters	Atom	x	y	z
Haeckelite	$Pmn2_1$	$a = 3.24$	Ga(2a)	0.50	0.18	0.44
		$b = 5.54$	N(2a)	0.50	0.82	0.44
		$c = 5.61$	Zn(2a)	0.50	0.81	0.08
		$\alpha = \beta = \gamma = 90$	O(2a)	0.00	0.69	0.91
Wurtzite	$P3m1$	$a = b = 3.24$	Ga(1a)	0.00	0.00	0.56
		$c = 5.30$	N(1a)	0.00	0.00	0.93
		$\alpha = \beta = 90$	Zn(1c)	0.67	0.33	0.46
		$\gamma = 120$	O(1c)	0.67	0.33	0.08

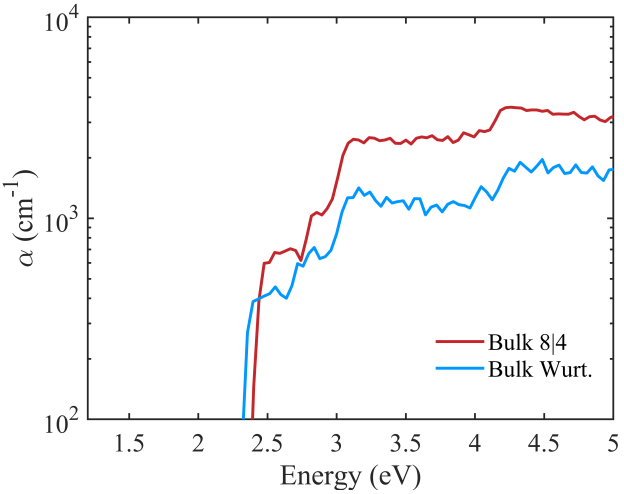

Fig. S1. HSE06 optical absorption coefficients for the bulk 8|4 and wurtzite phases by PWmat code.

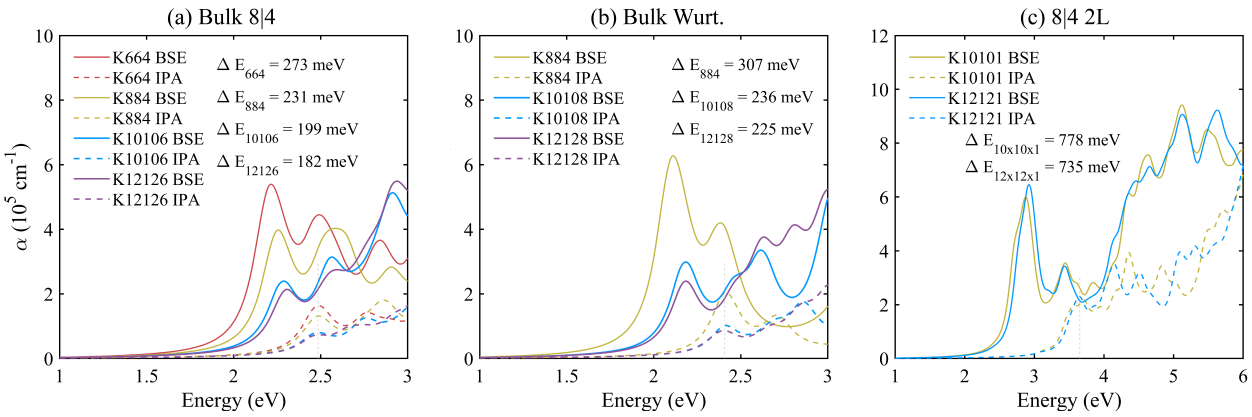

Fig. S2. The optical absorption spectra with (solid line) and without (dashed line) the electron-hole interaction in (a) bulk 8|4, (b) bulk wurtzite, and (c) two-layer 8|4 phases at the G_0W_0 approximation.

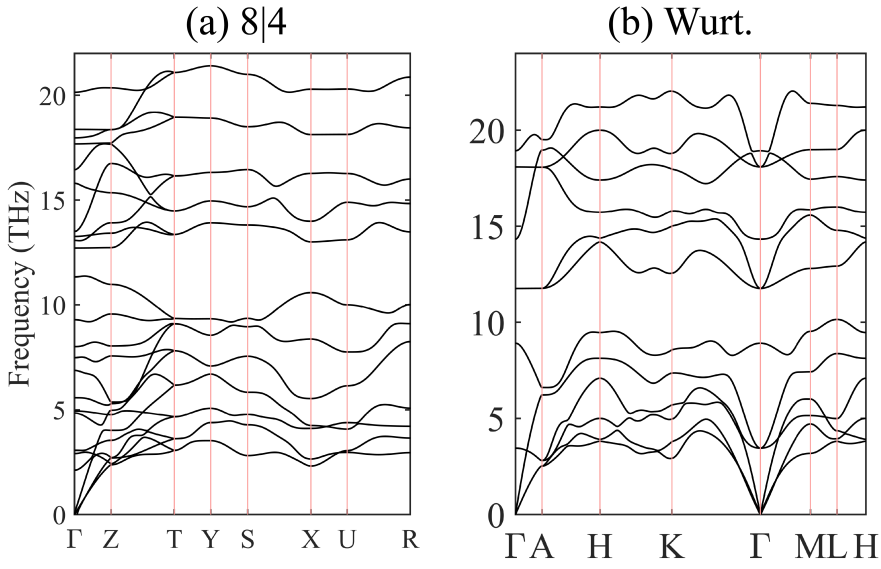

Fig. S3. Phonon spectra of bulk (a) haeckelite 8|4 and (b) wurtzite *P*3*m*1 $(GaN)_1(ZnO)_1$ alloys at ambient pressure.

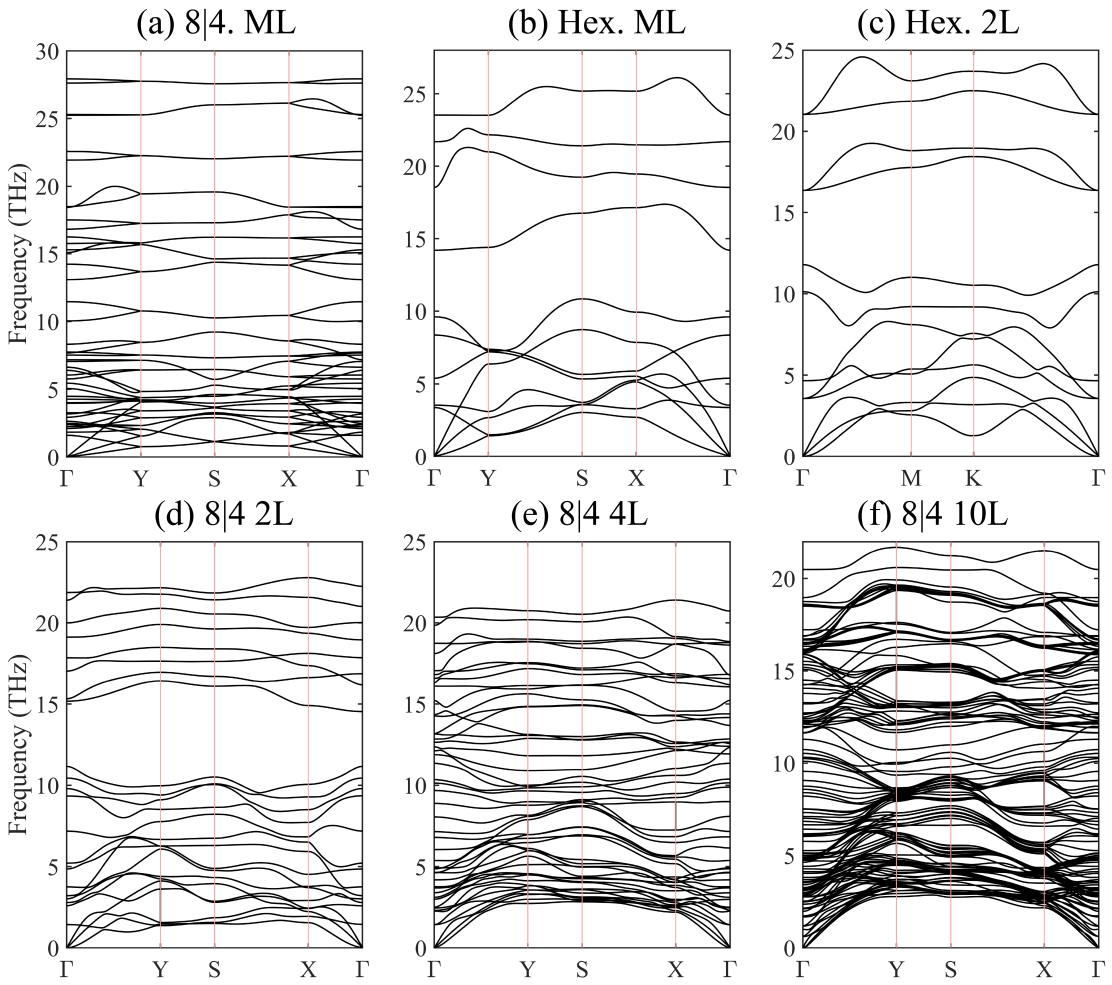

Fig. S4. Phonon spectra of (a) monolayer 8|4, (b) monolayer hexagonal, (c) two-layer hexagonal, (d) two-layer 8|4, (e) four-layer 8|4 and (f) ten-layer 8|4 configurations.

TABLE S2. Structural stability of two-, four- and six-layer wurtzite configurations with different stacking modes, where $\Delta E = E_{\text{Hex./Wurt.}} - E_{8|4}$.

	Configs./Stacking	E (eV/atom)	ΔE (meV/atom)
2L	8|4	-5.026	0
	Hex./AA	-4.973	53
	Hex./AB-1	-4.966	60
	Hex./AB-2	-4.969	57
4L	8|4	-5.111	0
	Wurt./AA	-4.968	143
	Wurt./ABAB	-4.958	153
6L	8|4	-5.152	0
	Wurt./AA	-5.036	116
	Wurt./ABBABB	-5.030	122

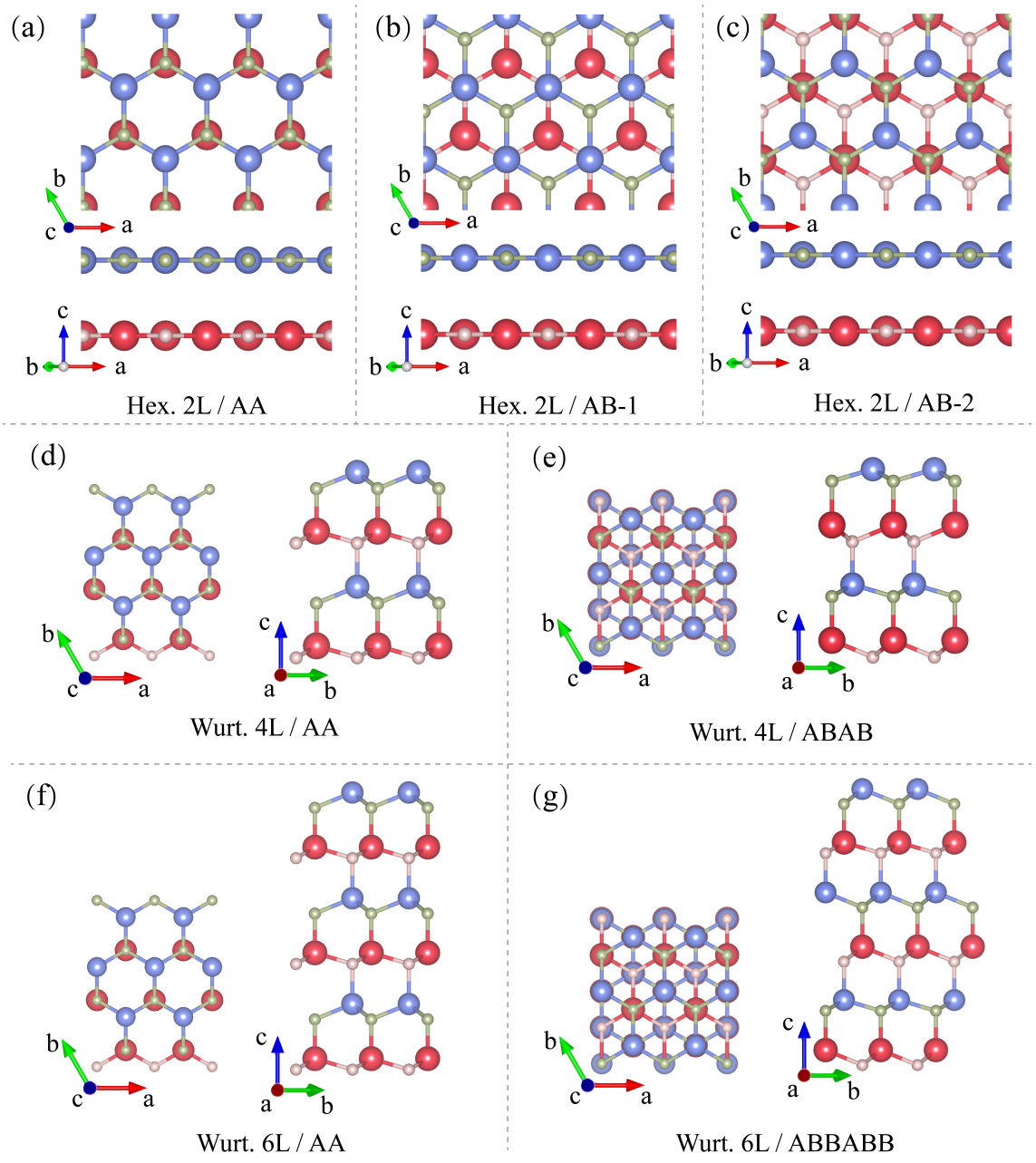

Fig. S5. Two-, four- and six-layer wurtzite configurations with different stacking modes.

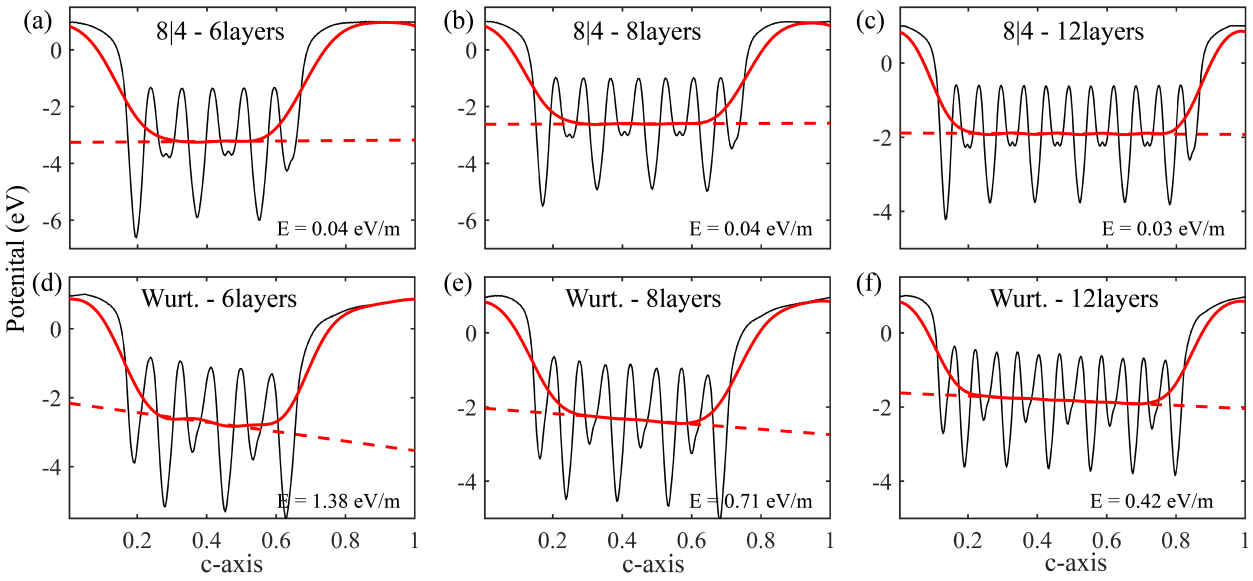

Fig. S6. Planar- (black line) and macroscopic-average (red line) internal electrostatic potentials along the *c* axis for six-, eight- and twelve-layer thicknesses in 8|4 and wurtzite configurations, respectively.

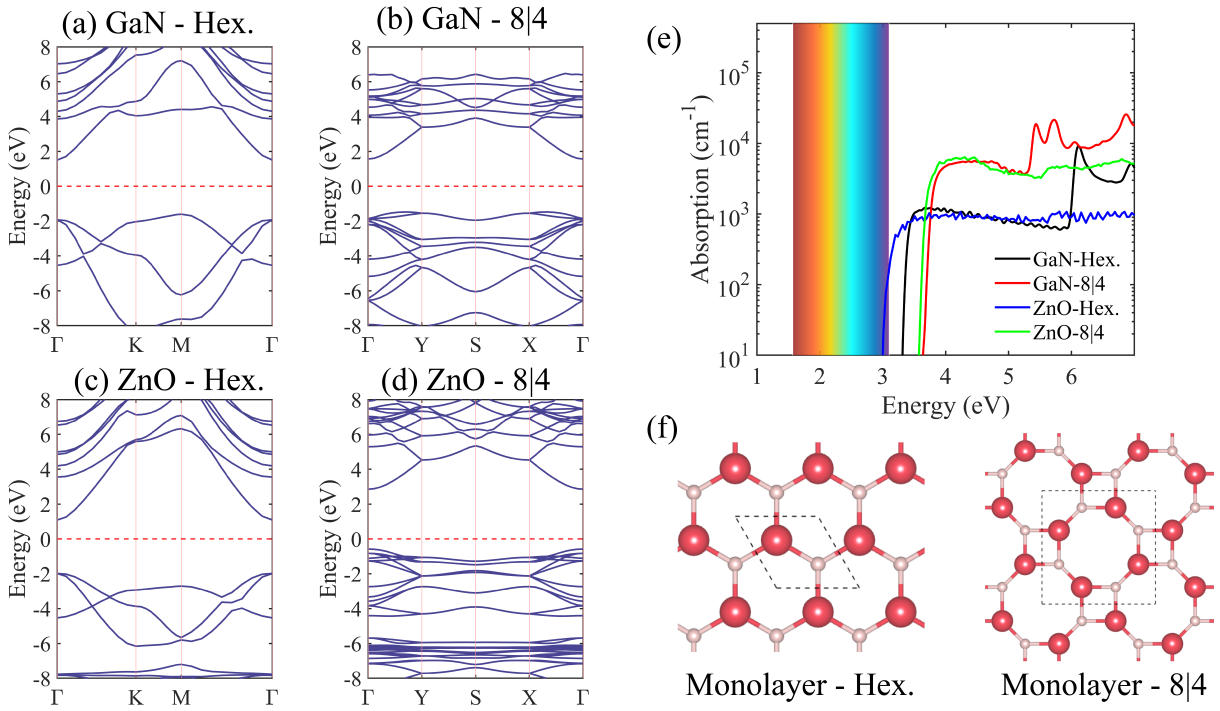

Fig. S7. HSE06 electronic band structures of monolayer planar hexagonal and 8|4 configurations: (a) hexagonal GaN, (b) 8|4 GaN, (c) hexagonal ZnO, (d) 8|4 ZnO. (e) Optical absorption coefficients for monolayer GaN and ZnO with hexagonal and 8|4 configurations. (f) Views of monolayer hexagonal and 8|4 configurations.

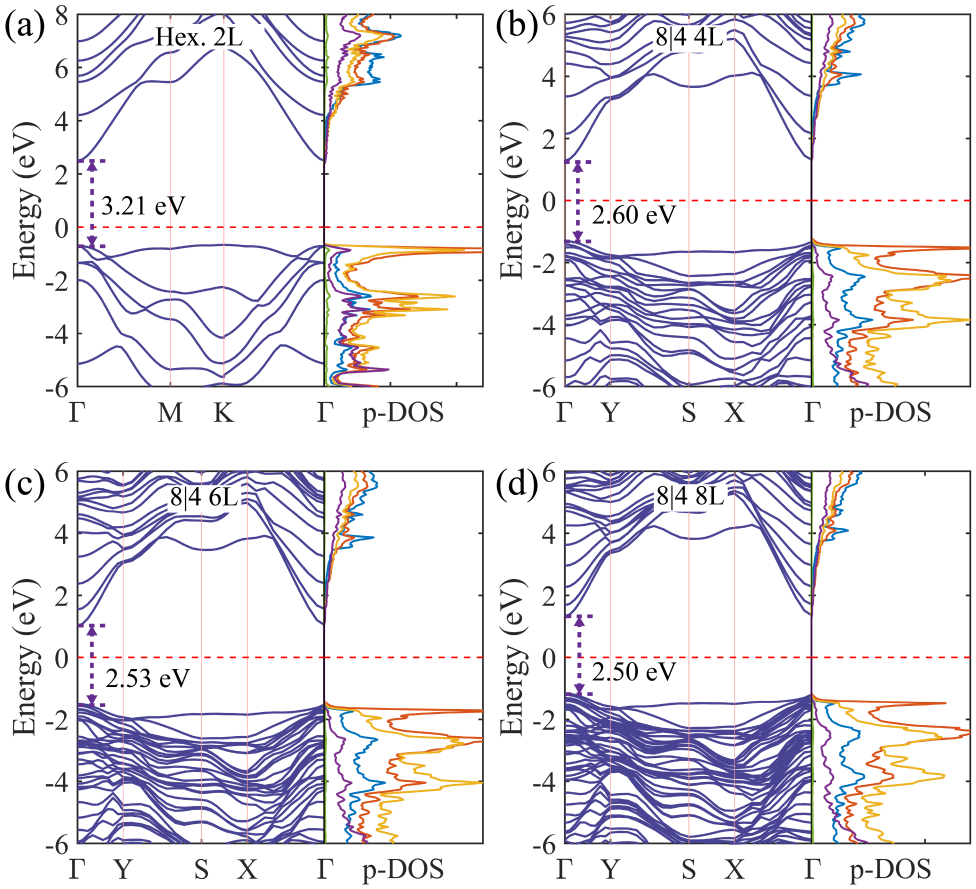

Fig. S8. HSE06 electronic band structures as well as densities of state of (a) two-layer hexagonal, (b) four-layer 8|4, (c) six-layer 8|4 and (d) eight-layer 8|4 configurations.

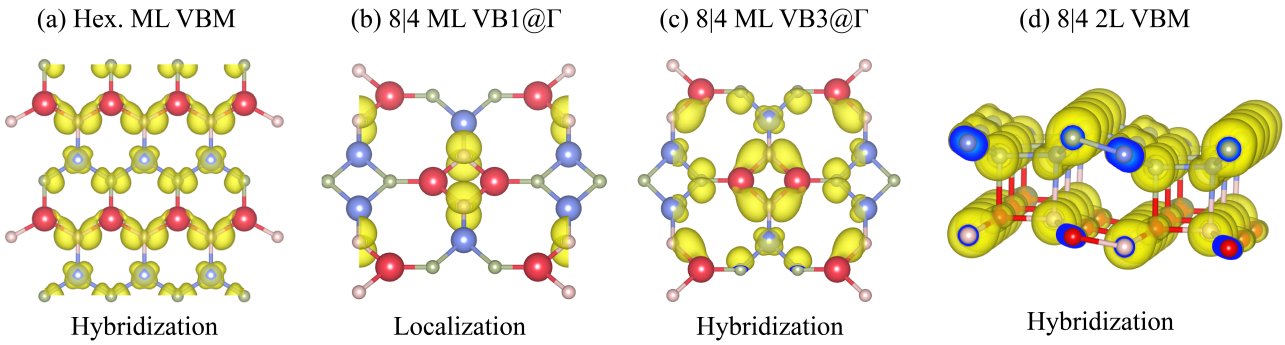

Fig. S9. Spatial valence band edge state distributions of (a) monolayer hexagonal, (b) and (c) monolayer 8|4, and (d) two-layer 8|4 configurations.

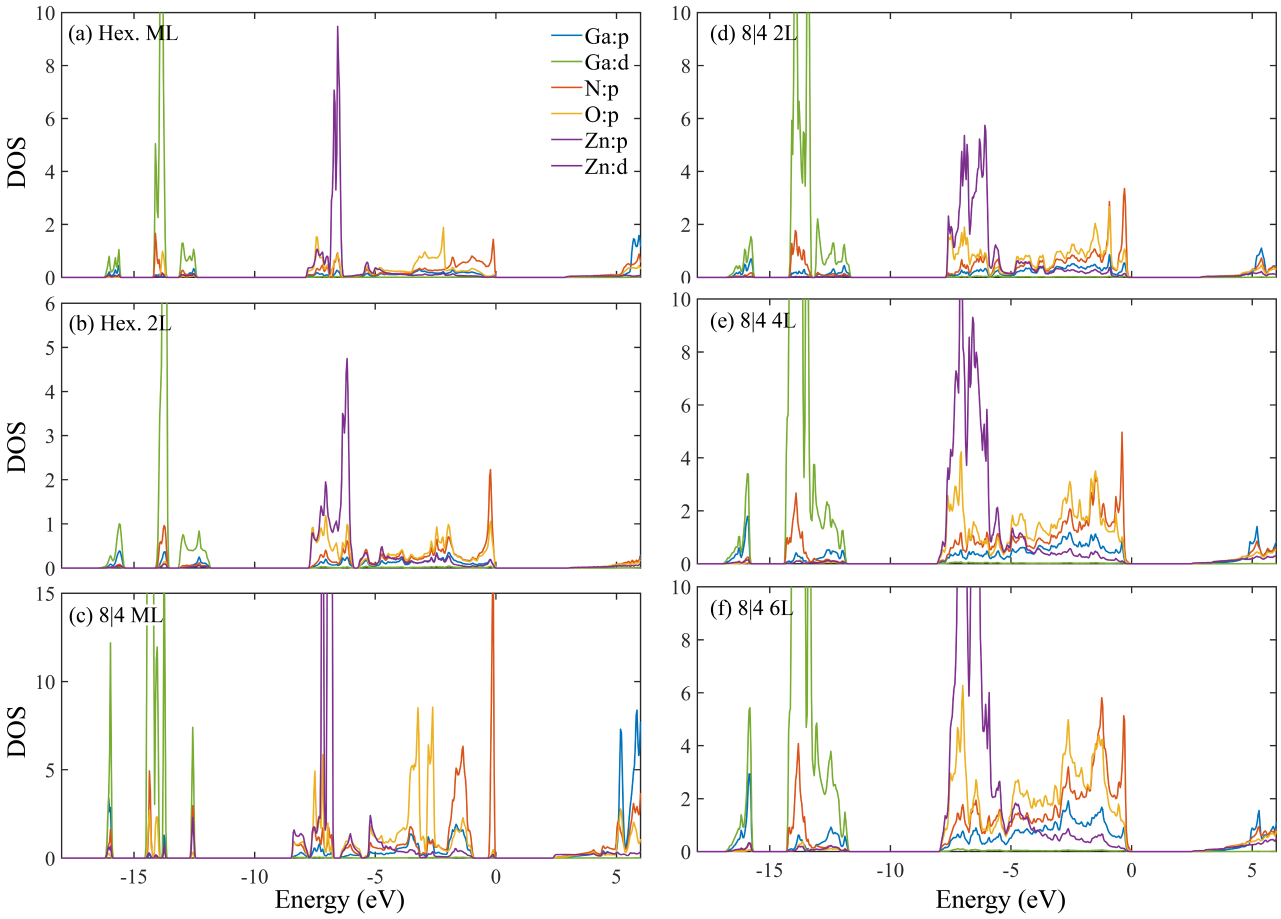

Fig. S10. HSE06 electronic densities of state of 2D configurations: (a) hexagonal monolayer, (b) hexagonal two layers, (c) 8|4 monolayer, (d) 8|4 two layers, (e) 8|4 four layers, and (f) 8|4 six layers.

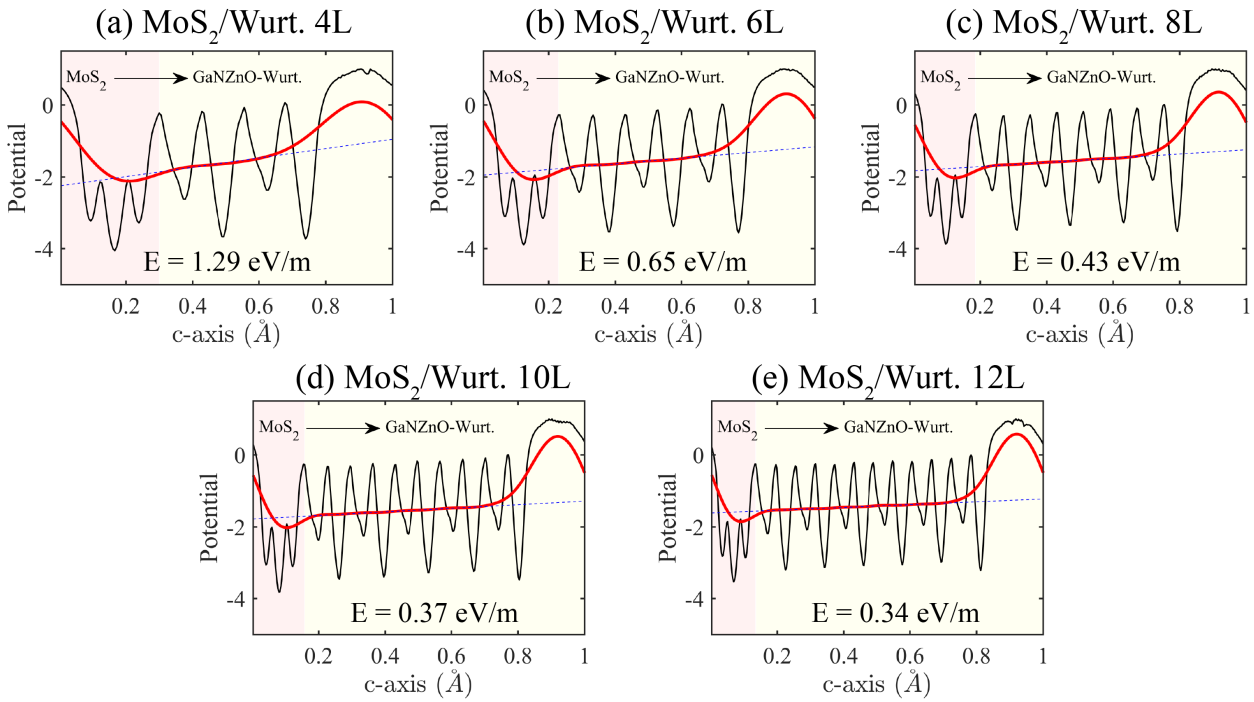

Fig. S11. Internal electrostatic potentials for MoS_2-based heterostructures with (a) four-, (b) six-, (c) eight-, (d) ten-, and (e) twelve-layer wurtzite configurations.

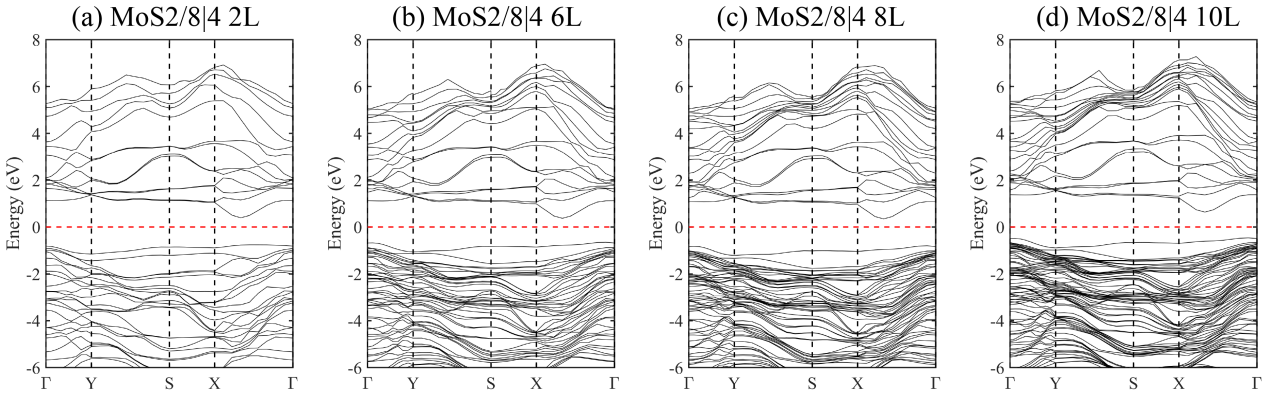

Fig. S12. HSE06 electronic band structure of MoS_2-based heterostructures with (a) two-, (b) six-, (c) eight-, and (d) ten-layer 8|4 configurations.